PCCP

PAPER

View Article Online
View Journal

Cite this: DOI: 10.1039/c5cp06726j

Theoretical study of electron tunneling through the spiral molecule junctions along spiral paths†

Xiaodong Xu,[a] Weiqi Li,[a] Xin Zhou,[b] Qiang Wang,[c] Jikang Feng,[d] Wei Quan Tian*[e] and Yongyuan Jiang*[a]

Received 4th November 2015,
Accepted 4th January 2016

DOI: 10.1039/c5cp06726j

www.rsc.org/pccp

The electronic transport properties of carbohelicenes and heterohelicenes absorbed between two metal electrodes have been investigated by using the nonequilibrium Green's function in combination with the density function theory. The transport properties of the molecular junctions are mainly dependent on the nature of spiral molecules. The detailed analyses of the transmission spectra, the energy levels as well as the spatial distribution of molecular projected self-consistent Hamiltonian explain how the geometry of molecules affects the intra-molecular electronic coupling. The spiral current in the configurations can be achieved by tuning the outer edge states of spiral-shaped molecules. Furthermore, the symmetric current–voltage characteristics are investigated with the bias changing for all devices as well as an negative differential resistance behavior is observed.

Introduction

Molecular-scale electronic devices have made remarkable progress and attracted much attention in recent years.[1,2] Plenty of molecules, especially single molecules, are expected to be used as functional building blocks in electronic devices because of their unique properties different from macroscopic systems. Since the concept of individual molecules as active electronic components was proposed,[3] molecular electronic devices have been accomplished experimentally and theoretically.[4,5] Numerous amazing characteristics have been proposed and realized, including rectifiers,[6–8] negative differential resistance[9], switches,[10–12] memory devices[13] and so on. Although tremendous progress has been made in the field of molecular devices, the fundamentals of electronic structure contributions of the building blocks to bulk transport still remains unclear.[14–16] It has been found that many factors can affect the electronic transport properties and rectifying performance, such as the coupling between molecules and electrodes,[17] the changing of molecular conformation with the applied bias,[18] spin-bias-induced charge currents,[19,20] *etc.* In essence, these can be attributed to the structure of molecular wires and the different transmission mechanisms.

Among a variety of functional molecules, helicene is a type of special molecule due to their unique spiral geometry, electronic structure and optical response properties.[21–24] Helicenes are polycyclic aromatic compounds with nonplanar spiral-shaped skeletons formed by ortho-fused benzene or other aromatic rings that are endowed with helical chirality. It is the inherently dissymmetric backbone that makes helicenes structurally intriguing for application in the areas of molecular machines, liquid crystal technology and molecular recognition. In addition, their helical topology combined with extended π-conjugated systems can bring strong responses in electronic circular dichroism. A large number of spiral-shaped molecules, such as DNA,[25,26] carbohelicenes,[27] heterohelicenes,[28–32] *etc.*, have been discovered and fabricated in biology and chemistry. As a consequence, there has been increasing interest and research activity in this field and enormous progress has been made in recent decades.

External stimuli, such as light field,[33–35] mechanical force[36–38] and magnetic field,[39] can be introduced to modulate the molecular conductivity and thus to tune the properties of functional molecular devices. Helicenes, which combine the special optical response[40,41] and quantum transport properties,[42,43] might have great potential application in molecular electronics. Under nonequilibrium conditions, the junctions might generate spiral current due to molecular spiral geometry which can be used as nano-solenoid-coils to create magnetic field. Though the accurate simulation of the magnetic field of helical nano-structures cannot be achieved at the present level of theory,

[a] Department of Physics, Harbin Institute of Technology, Harbin, 150001, P. R. China. E-mail: jiangyy@hit.edu.cn
[b] Institute of Theoretical and Simulational Chemistry, Academy of Fundamental and Interdisciplinary Sciences, Harbin Institute of Technology, Harbin, 150001, P. R. China
[c] Department of Applied Chemistry, College of Science, Nanjing Tech University, Nanjing, 211816, P. R. China
[d] Institute of Theoretical Chemistry and College of Chemistry Jilin University, 130023, Changchun, P. R. China
[e] College of Chemistry and Chemical Engineering, Chongqing University, Chongqing 400044, P. R. China

† Electronic supplementary information (ESI) available. See DOI: 10.1039/c5cp06726j

some studies show that the magnetic field can be produced in the external electric field of molecules or nano-structures. For example, Barth *et al.* predicted that electron ring currents and induced magnetic fields have been driven in atoms and molecules by circularly polarized laser pulses.[44,45] Recently, Xu *et al.* used the tight-binding (TB) method in combination with the non-equilibrium Green's function (NEGF) to predict the magnetic field in some spiral nano-structures.[46,47] However, the studies on the electronic properties of helicenes are rare. In the present work, the electronic transport properties of certain classical helicenes will be investigated in detail. Incorporating the properties of the transmission spectra, the energy levels, the spatial distribution of molecular projected self-consistent Hamiltonian (MPSH) as well as local transmission pathways, the transport mechanism of these helicenes will be revealed.

Models and calculation methods

To investigate the electronic transport properties of spiral-shaped molecules coupled to metal electrodes, three molecules composed of carbohelicenes and two thiol-[7]helicenes with benzenethiolates at both sides were designed, which were marked as S1, S2 and S3, respectively (as shown in Fig. 1). For single molecular junctions, gold is the most popular to be used as electrodes and the thiol group is suitable as an anchoring group due to the strong bonding between the sulfur atom and the gold surface.[48–50] Spiral-shaped molecules were coupled with two Au(111) surfaces, represented by a (5×5) supercell with periodic boundary conditions in this work.

The geometry of all spiral molecules was firstly optimized at the B3LYP/6-31G* theoretical level by using the Gaussian 03 software,[51] and the optimized molecules were sandwiched between two metal electrodes as shown in Fig. 2. All systems were completely optimized until the absolute force on each atom was less than 0.1 eV Å^{-1}. The electronic transport properties of the molecular junctions were predicted using the NEGF combined with the density functional theory (DFT) method as implemented in ATK software package[52–55] using the double-zeta plus polarization basis set for molecule atoms and single-zeta plus polarization basis set for electrode atoms. The GGA-PBE (generalized gradient approximation using the Perdew–Burke–Ernzerhof parameterization) was utilized as the exchange and correlation functional for all calculations of electron–electron interactions.[56] The mesh energy cutoff of real space for three junctions was tested accurately until the energy changed below 10^{-3} eV and 150Ry was finally chosen to balance the efficiency and the accuracy for electronic transport calculations. The Brillouin zone of all molecular junctions was sampled using $5 \times 5 \times 100$ points to improve the calculation accuracy. The current through the molecular junctions was calculated by utilizing the Landauer–Büttiker formula:[57,58]

$$I(V) = \frac{2e}{h}\int T(E, V_b)[f(E-\mu_L) - f(E-\mu_R)]\mathrm{d}E$$

where $f(E)$ is the Fermi distribution function, h is Planck's constant, e is electron charge, $\mu_{L(R)}$ is the chemical potential of the left(right) electrode where $\mu_L = E_F + eV/2$, $\mu_R = E_F - eV/2$. E_F, the Fermi level of the system is set to be zero in calculations and $T(E, V_b)$ is the transmission coefficient under different biases obtained using the following formula:

$$T(E, V_b) = T_r[\Gamma_L(E)G^R(E)\Gamma_R(E)G^A(E)]$$

where $G^{R(A)}(E)$ is the retarded or advanced Green's function. $\Gamma_{L(R)}(E)$ is the coupling function between molecules and electrodes.

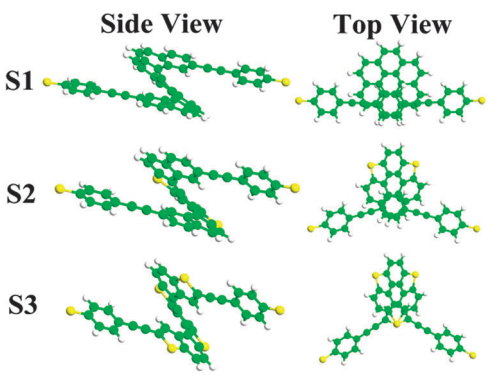

Fig. 1 Schematic structures of the spiral-shaped molecules, marked as S1, S2 and S3. The left (right) hand of the sketch map represents the side (top) view of the three molecules. The green, yellow and white balls represent carbon, sulfur and hydrogen atoms, respectively. The differences among them are presented at the outer edges of the center section, while they have the same anchoring groups. At the center section, molecule S1 is made up of carbon-[7]helicene, while molecule S2 includes five ortho-fused benzenes as well as two thiophenes, and S3 is made up of three ortho-fused benzenes and four thiophenes.

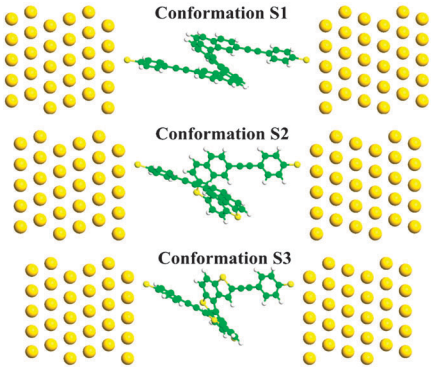

Fig. 2 Geometries of the metal–molecule–metal junctions. The spiral-shaped molecules are sandwiched between two metallic surfaces of gold. The models of the two-electrode junctions are divided into three regions, including the left electrode, scattering region, and right electrode. The sulfur atoms on the both sides of molecules are located at the hollow site on the metallic surfaces.

Results and discussion

The equilibrium transport properties of these three molecular junctions under zero bias are shown in Fig. 3(a). In the energy region considered for all structures, the first peak of the

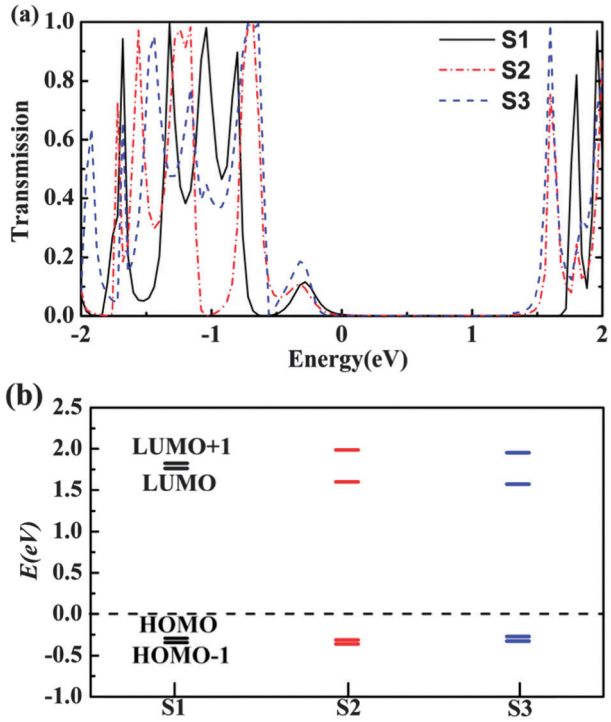

Fig. 3 (a) Transmission spectra of the three molecular junctions at zero bias and the Fermi level is set to zero. The black solid, red dashed dot and blue dashed line represent the transmission curve of S1, S2 and S3, respectively. (b) The distribution of the LUMO+1, LUMO, HOMO and HOMO−1 energy levels for the three molecules.

transmission spectra under the Fermi level, contributed by the highest occupied molecular orbital (HOMO) and the second occupied molecular orbital(HOMO−1) together, play the major role in electronic transmission, while the peak contributed by the lowest unoccupied molecular orbital (LUMO) is far away from the Fermi level. The transmission coefficients of structure S3 at the HOMO and HOMO−1 resonance peaks under zero bias are larger than that of S1 and S2. Moreover, the transmission spectra also present some differences in the position and density of peaks because of the difference of the intra-molecular electronic coupling among the three molecular junctions. These shifts of transmission peaks can be observed clearly in the molecular orbital energy levels as shown in Fig. 3(b). For molecules S1, S2 and S3, the gap between the HOMO and LUMO is 2.05 eV, 1.91 eV and 1.84 eV, respectively, and the HOMO−1 lies very close to the HOMO displaying remarkable electronic couplings for charge transport. As a result, the significant transmission peak near the Fermi level is contributed by the HOMO and HOMO−1 bands together. In addition, the gap between the LUMO and LUMO+1 for structures S2 and S3 is larger than S1 at zero bias.

To analyze the transport mechanism, the spatial distribution of MPSH is calculated, as exhibited in Fig. 4. The position of transmission peak is generally determined by the energy levels of MPSH and the value of transmission peak height is dependent on the delocalization of molecular orbitals.[41] The HOMO−1 and HOMO are delocalized over the framework of molecules which provide good channels for electron tunneling through the molecular junctions and lead to a significant transmission peak for structures S2 and S3. For S1, the orbital spatial distribution of the HOMO and HOMO−1 is mainly delocalized on the two branches of molecules, which primarily determines the channel of charge tunneling in the interlayer. Besides, the LUMO and LUMO+1 are mainly delocalized at central part of all spiral-shaped molecules. Comparing the LUMO and LUMO+1 of S3 with the other two molecules, the delocalized electronic density extends to the two terminal sulfur atoms. It indicates that stronger coupling exists between the molecules and electrodes and leads to a higher LUMO transmission peak[59] in correspondence with transmission curves. As mentioned above, due to various properties of the transmission spectra, the energy levels and the electronic structures, unique electronic transport properties are expected for these molecules.

To study the influence of geometry on electron tunneling through the junctions, the local transmission pathways in molecules have been calculated.[60,61] The local transmission pathways of these three molecular junctions at the HOMO (or HOMO−1) energy level with the same threshold at zero bias are shown in Fig. 5. The local transmission is represented by the distribution of arrows on the molecules and the colors stand for the angle of the transport directions. For molecule S1,

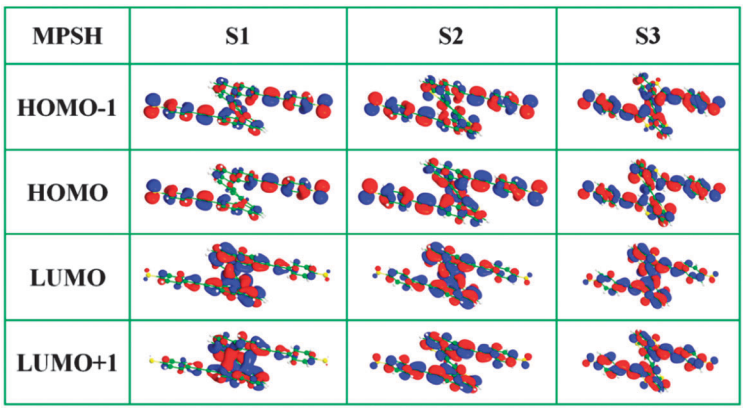

Fig. 4 The spatial distribution of the frontier molecular orbital for three molecular junctions at zero bias. The isovalue is set to 0.06 for all plots.

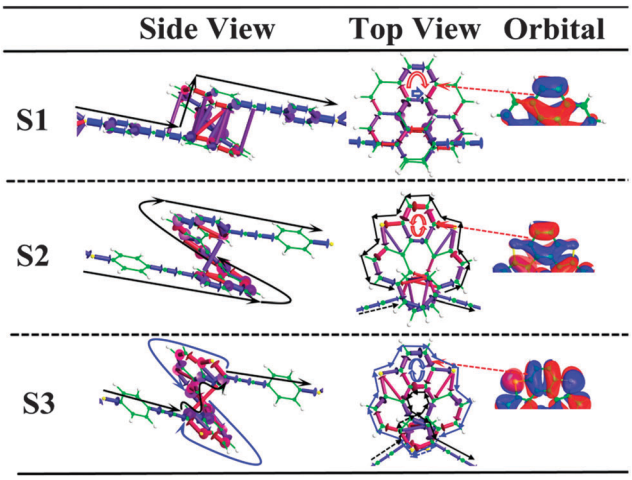

Fig. 5 The local transmission pathways through S1, S2 and S3 at the HOMO energy level under zero bias. The left (central) part of the sketch map represents the side (top) view of the local transmission. The right part shows the HOMO distributed on the top hexagon of the top view of these spiral molecules. The lines with arrows indicate the directions of the current.

there is no spiral current flowing through the molecular junction at this energy level, and the total current is offered primarily by tunneling electrons from the top layer to the bottom layer. Obviously, a local loop current (see the top view of S1) which is in the clockwise direction is observed on the top hexagon of S1 molecule, caused by the HOMO distributing on this ring. However, there is an evident spiral current flowing through the molecular junction which appears at the outer edge of molecule S2 along the anticlockwise direction marked with the black line. The tunnelling current in the interlayer is also presented while it is only a small contribution to transmission. On the other hand, a local anticlockwise loop current appears on the top hexagon of molecule S2. This is due to a tunneling channel on this ring presented by the HOMO. Importantly, the direction of the loop current depends on the direction of the spiral current at the outer edge. More interestingly, there are two tracks of spiral current presented in molecule S3, but the transport directions are opposite to each other. One of the spiral currents flowing from high potential to low potential transports through the molecule at the inner edge in the anticlockwise direction labelled with the black line and the other flowing to high potential transports through the molecule at the outer edge in the clockwise direction labelled with the blue line. Similarly, molecule S3 has a local loop current which is in the clockwise direction and tunnelling current in the interlayer. We can draw a semblable consequence that the loop current is caused by the HOMO localized on the top hexagon of these molecules and its direction is determined by the direction of spiral current at edges. Not only spiral current but also local loop current can be expected to generate magnetic field. One of the reasons for the different transmission pathways is the distance between the top and the bottom aromatic rings of spiral molecules, and the distance of the nearest atoms between layers for S1, S2 and S3 is 3.0 Å, 3.14 Å, and 3.21 Å, respectively. Namely, a small interlayer distance increases the chance of interlayer

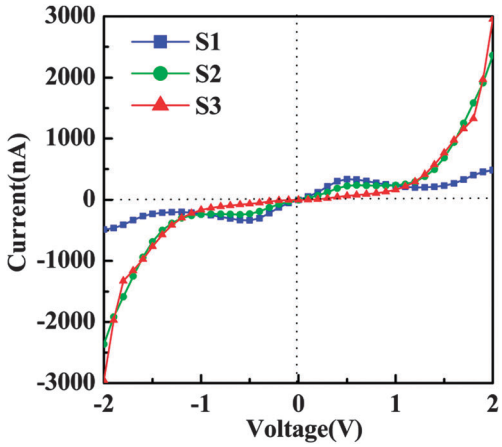

Fig. 6 The current–voltage curves of the molecular junctions with the bias ranging from −2 V to 2 V. The blue square line, green circle line and red triangle line indicate S1, S2 and S3 molecular junctions, respectively.

electron tunneling. Moreover, directed electron circulation may produce an induced magnetic field, which makes these structures suitable for special application in molecular devices, for example, nano-solenoid-coil.

From the features of the current through the molecular junctions under nonequilibrium conditions, more about the transport properties of the three structures can be revealed. Fig. 6 exhibits the current–voltage (I–V) curves of the molecular junctions with bias ranging from −2.0 V to 2.0 V. Under positive or negative bias, the current–voltage curves have the same trend of variation for every molecule, and the transport properties of the devices are strongly dependent on the variety of molecules. For example, as shown in Fig. 6, when the bias voltage increases from 0.0 V to 0.5 V, the current will increase gradually for all structures. However, with the voltage increasing from 0.5 V to 1.1 V the current in S1 and S2 decreases slightly, while the current of S3 still remains increasing. The current value with the bias voltage ranging from 0.0 V to 1.1 V follows the order S1 > S2 > S3, in line with the transmission spectra. The reasons for these behaviors are all rooted in the transmission peak of S1 near the Fermi level has a bigger section entering the bias window, which primarily makes a contribution to current integral.

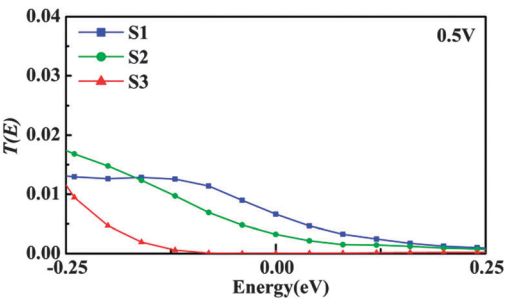

Fig. 7 The portion of transmission spectra located in the bias window at 0.5 V voltage. The bias window ranges from −0.25 eV to 0.25 eV, and the blue square, green circle and red triangle line indicate S1, S2 and S3, respectively.

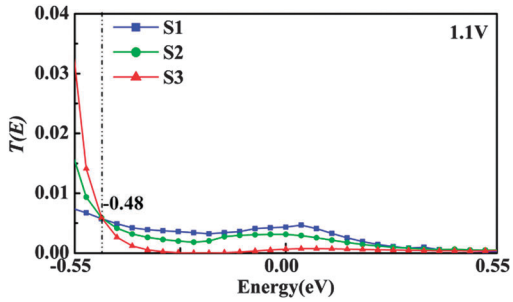

Fig. 8 The portion of transmission spectra located in the bias window at 1.1 V voltage. The bias window ranges from −0.55 eV to 0.55 eV, and the blue square, green circle line and red triangle line indicate S1, S2 and S3, respectively.

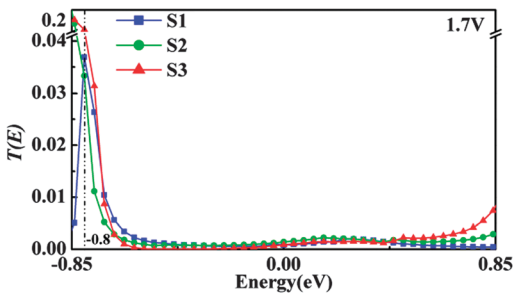

Fig. 9 The portion of transmission spectra located in the bias window at 1.7 V voltage. The bias window ranges from −0.85 eV to 0.85 eV, and the blue square, green circle and red triangle line indicate S1, S2 and S3, respectively.

More interestingly, the three current–voltage curves have an intersection near a bias voltage of 1.1 V. With the bias further increasing, the current in S2 and S3 rapidly increases, while S1 still keeps dropping until the bias voltage exceeds 1.4 V. To describe the current trend in detail, applied biases at 0.5 V, 1.1 V and 1.7 V were chosen. It is well known that current is determined by the integral of the portion of transmission entering the bias window. Under 0.5 V bias, the bias window ranges from −0.25 eV to 0.25 eV, the portion of transmission spectra entering the bias window is presented in Fig. 7. It is obvious to observe that the relationship of the transmission spectra in this bias window is $T(S1) > T(S2) > T(S3)$ which leads a current value order $I(S1) > I(S2) > I(S3)$. Fig. 8 shows the transmission spectra with the bias window ranging −0.55 eV to 0.55 eV under 1.1 V bias and the order of transmission spectra of these molecular junctions is $T(S1) > T(S2) > T(S3)$ in the [−0.55 eV, −0.48 eV] energy region, while the order gets reversed in [−0.48 eV, 0.55 eV] energy region. The integral of transmission spectra of these molecular junctions finally leads to a similar value of current. In Fig. 9, transmission spectrum of S1 is much lower than S2 and S3 in the [−0.85 eV, −0.8 eV] energy region which determines the order of the transmission spectra approximating to $T(S3) \approx T(S2) \gg T(S1)$ and the integral of transmission spectra finally gets a current order $I(S3) \approx I(S2) > I(S1)$ at 1.7 V bias. According to analyses above, the transport properties of these molecular junctions can be understood deeply.

Another interesting phenomenon shown in *I–V* curves is the negative differential resistance behavior (called NDR as well) in configurations S1 and S2. To understand NDR of these molecular junctions clearly, the transmission spectra and the corresponding PDOS (projected density of states) at 0.5 V, 0.8 V, and 1.1 V biases are analyzed in detail, as presented in Fig. 10. Because the PDOS gives information of the molecular orbital contributing to the eigenstate of the junctions and the transmission reveals a clear correspondence to the PDOS, the mechanism of the NDR can be expounded by the evolution of the PDOS and transmission spectra in bias windows. For S1 (Fig. 10(a)), obviously, there is a big part of the transmission spectrum entering the bias window at 0.5 V bias. As the bias increases from 0.5 V to 0.8 V, the portion of the transmission spectrum in the bias window exhibits a decrease caused by the PDOS. As a result, a decrease appears in current. When bias increases further, the strength of the transmission spectrum in the bias window becomes weaker leading to a decrease in

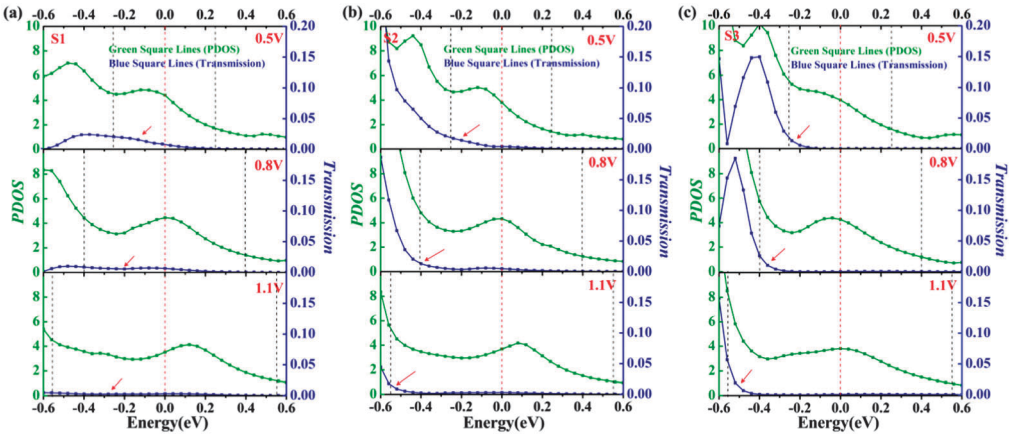

Fig. 10 The changes in transmission spectra and corresponding PDOS of molecular junctions S1, S2 and S3 under bias voltages of 0.5 V, 0.8, and 1.1 V. The green and blue square lines represent the corresponding PDOS and the transmission spectra, respectively. The black dashed lines indicate the bias window and red dashed lines the Fermi level.

current as well. Namely, an NDR behavior occurs in molecular junction S1. Similarly, there is a decrease in current with the bias increasing from 0.5 V to 1.1 V consistent with the evolution of the transmission spectrum and PDOS, as shown in Fig. 10(b). It indicates that an NDR behavior also appears in molecular junction S2. Interestingly, a sharp contrast to S1 and S2 is that there is no NDR behavior observed in the current–voltage correlation of molecular junction S3, presented by the sustainable growth of the transmission spectra and PDOS in the bias windows from 0.5 V to 1.1 V, as shown in Fig. 10(c).

Further investigation has been conducted on the influence of the self-interaction on the electronic transport properties of these spiral molecules. The disagreement of the transport properties of molecular junctions between the theory and experiment remains large, even for simple molecules, some other influence factors should be been taken into account, such as electrodes,[62] the position of molecules,[63] anchoring groups[64] and the self-interaction of molecules[65] and so on. Many investigations have confirmed that the theoretical predictions are in much closer agreement with experiments when self-interaction corrected exchange and correlation functionals are employed.[66,67] The GGA+U approach was employed to investigate the influence of the self-interaction on molecular junction S2. As a result, the transport properties are primarily affected by the self-interaction. The modulation of current can be predicted by transmission spectra with different corrections of U (see ESI†). In addition, the spiral current at the outer edges of molecule S2 always exists and some other tunneling channels are opened with the value of U increasing (shown in Fig. S1, ESI†). As the systematic error of the method exists in all predictions of these systems, the variation pattern of electro-magnetic properties would be similar if self-interaction correction is taken into account.

Conclusions

In summary, the electronic transport properties of spiral-shaped molecules sandwiched between gold electrodes have been studied by the first principles calculations. The spiral-shaped molecules have a similar spiral geometry but different components leading to their unique electronic properties. There is no spiral current flowing through molecule S1 and the total current is only offered by electron tunneling in the interlayer. When the thiophene rings are introduced in helicenes like molecules S2 and S3, molecular conformations and electron distribution of frontier orbitals will vary, and the spiral current appears, which provides the possibility to generate magnetic field. The local loop current observed in molecules S2 and S3 is caused by the molecular orbital distribution, and its direction is primarily dependent on the direction of the spiral current at the edges. In addition, the current–voltage curves indicate that an NDR behavior occurs in structures S1 and S2 but not in S3. At low bias, the order of current among three structures is S1 $>$ S2 $>$ S3. With the bias increasing further, the order will shift to S1 $\ll$ S2 $\approx$ S3, meaning that the shift of the current–voltage curves presents a switching effect. The present work provides useful information on the application of spiral-shaped molecules in the field of molecule solenoids and other functional components.

Acknowledgements

This work was supported by the Natural Science Foundation of China under grant number (11104048, 21303030, 21203094, and 21373112), and the Open Project of State Key Laboratory of Supramolecular Structure and Materials (JLU) (SKLSSM2015018).

References

1 A. Nitzan and M. A. Ratner, *Science*, 2003, **300**, 1384–1389.
2 C. Huang, A. V. Rudnev, W. Hong and T. Wandlowski, *Chem. Soc. Rev.*, 2015, **44**, 889–901.
3 A. Aviram and M. A. Ratner, *Chem. Phys. Lett.*, 1974, **29**, 277–283.
4 M. Paulsson, T. Frederiksen and M. Brandbyge, *Nano Lett.*, 2006, **6**, 258–262.
5 H. Rascón-Ramos, J. M. Artés, Y. Li and J. Hihath, *Nat. Mater.*, 2015, **14**, 517–522.
6 A. Martin, J. Sambles and G. Ashwell, *Phys. Rev. Lett.*, 1993, **70**, 218.
7 J. Taylor, M. Brandbyge and K. Stokbro, *Phys. Rev. Lett.*, 2002, **89**, 138301.
8 H. Liu, Y. He, J. Zhang, J. Zhao and L. Chen, *Phys. Chem. Chem. Phys.*, 2015, **17**, 4558–4568.
9 J. Chen, M. Reed, A. Rawlett and J. Tour, *Science*, 1999, **286**, 1550–1552.
10 J. L. Zhang, J. Q. Zhong, J. D. Lin, W. P. Hu, K. Wu, G. Q. Xu, A. T. Wee and W. Chen, *Chem. Soc. Rev.*, 2015, **44**, 2998–3022.
11 J. Taylor, M. Brandbyge and K. Stokbro, *Phys. Rev. B: Condens. Matter Mater. Phys.*, 2003, **68**, 121101.
12 J. Zhao, W. Zhao, B. Cui, C. Fang, Y. Xu, X. Kong, D. Li and D. Liu, *RSC Adv.*, 2014, **4**, 40941–40950.
13 M. Reed, J. Chen, A. Rawlett, D. Price and J. Tour, *Appl. Phys. Lett.*, 2001, **78**, 3735–3737.
14 M. Di Ventra, S. Pantelides and N. Lang, *Phys. Rev. Lett.*, 2000, **84**, 979.
15 S. M. Lindsay and M. A. Ratner, *Adv. Mater.*, 2007, **19**, 23–31.
16 M. A. Reed, C. Zhou, C. Muller, T. Burgin and J. Tour, *Science*, 1997, **278**, 252–254.
17 V. V. Zhirnov and R. K. Cavin, *Nat. Mater.*, 2006, **5**, 11–12.
18 W. Haiss, C. Wang, I. Grace, A. S. Batsanov, D. J. Schiffrin, S. J. Higgins, M. R. Bryce, C. J. Lambert and R. J. Nichols, *Nat. Mater.*, 2006, **5**, 995–1002.
19 F. Zhai, X. Zhao and H. Xu, *Appl. Phys. Lett.*, 2009, **94**, 262103.
20 Q. Wu, P. Zhao, Y. Su, S. Li, J. Guo and G. Chen, *RSC Adv.*, 2015, **5**, 52938–52944.
21 A. Bossi, E. Licandro, S. Maiorana, C. Rigamonti, S. Righetto, G. R. Stephenson, M. Spassova, E. Botek and B. Champagne, *J. Phys. Chem. C*, 2008, **112**, 7900–7907.
22 B. Jansík, A. Rizzo, H. Ågren and B. Champagne, *J. Chem. Theory Comput.*, 2008, **4**, 457–467.

23 A. Rajca, M. Pink, S. Xiao, M. Miyasaka, S. Rajca, K. Das and K. Plessel, *J. Org. Chem.*, 2009, **74**, 7504–7513.
24 J. Heurich, J. Cuevas, W. Wenzel and G. Schön, *Phys. Rev. Lett.*, 2002, **88**, 256803.
25 D. Klotsa, R. A. Römer and M. S. Turner, *Biophys. J.*, 2005, **89**, 2187–2198.
26 C. Dekker and M. A. Ratner, *Phys. World*, 2001, **14**, 29–33.
27 R. Martin and M. Baes, *Tetrahedron*, 1975, **31**, 2135–2137.
28 H. Oyama, K. Nakano, T. Harada, R. Kuroda, M. Naito, K. Nobusawa and K. Nozaki, *Org. Lett.*, 2013, **15**, 2104–2107.
29 K. Nakano, H. Oyama, Y. Nishimura, S. Nakasako and K. Nozaki, *Angew. Chem.*, 2012, **124**, 719–723.
30 P. Sehnal, I. G. Stará, D. Šaman, M. Tichý, J. Míšek, J. Cvačka, L. Rulíšek, J. Chocholoušová, J. Vacek and G. Goryl, *Proc. Natl. Acad. Sci. U. S. A.*, 2009, **106**, 13169–13174.
31 M. Miyasaka, A. Rajca, M. Pink and S. Rajca, *J. Am. Chem. Soc.*, 2005, **127**, 13806–13807.
32 C. E. Szakacs and P. G. Mezey, *J. Phys. Chem. A*, 2008, **112**, 6783–6787.
33 W. R. Browne and B. L. Feringa, *Annu. Rev. Phys. Chem.*, 2009, **60**, 407–428.
34 I. L. Fabelinskii, *Molecular scattering of light*, Springer Science & Business Media, 2012.
35 K. Takahashi, H.-B. Cui, Y. Okano, H. Kobayashi, Y. Einaga and O. Sato, *Inorg. Chem.*, 2006, **45**, 5739–5741.
36 X. Cui, A. Primak, X. Zarate, J. Tomfohr, O. Sankey, A. Moore, T. Moore, D. Gust, G. Harris and S. Lindsay, *Science*, 2001, **294**, 571–574.
37 B. I. Yakobson and R. E. Smalley, *Am. Sci.*, 1997, 324–337.
38 K. C. Neuman and A. Nagy, *Nat. Methods*, 2008, **5**, 491–505.
39 F. Schedin, A. Geim, S. Morozov, E. Hill, P. Blake, M. Katsnelson and K. Novoselov, *Nat. Mater.*, 2007, **6**, 652–655.
40 E. Botek, J.-M. André, B. Champagne, T. Verbiest and A. Persoons, *J. Chem. Phys.*, 2005, **122**, 234713.
41 E. Botek, B. Champagne, M. Turki and J.-M. André, *J. Chem. Phys.*, 2004, **120**, 2042–2048.
42 G. L. Zhang, H. L. Yuan, H. Zhang, Y. Shang and M. Sun, *Int. J. Quantum Chem.*, 2011, **111**, 4214–4223.
43 G. Zhang, D. Li, Y. Shang, H. Zhang, M. Sun, B. Liu and Z. Li, *J. Phys. Chem. C*, 2011, **115**, 5257–5264.
44 I. Barth and J. Manz, *Phys. Rev. A: At., Mol., Opt. Phys.*, 2007, **75**, 012510.
45 I. Barth, L. Serrano-Andrés and T. Seideman, *J. Chem. Phys.*, 2008, **129**, 164303.
46 F. Xu, A. Sadrzadeh, Z. Xu and B. I. Yakobson, *Comput. Mater. Sci.*, 2014, **83**, 426–433.
47 F. Xu, H. Yu, A. Sadrzadeh and B. I. Yakobson, *Nano Lett.*, 2015, DOI: 10.1021/acs.nanolett.5b02430.
48 W. Andreoni, A. Curioni and H. Grönbeck, *Int. J. Quantum Chem.*, 2000, **80**, 598–608.
49 M. Ford, R. Hoft and J. Gale, *Mol. Simul.*, 2006, **32**, 1219–1225.
50 F. Tielens and E. Santos, *J. Phys. Chem. C*, 2010, **114**, 9444–9452.
51 M. J. Frisch, G. W. Trucks, H. B. Schlegel, G. E. Scuseria, M. A. Robb, J. R. Cheeseman, J. A. Montgomery, Jr., T. Vreven, K. N. Kudin, J. C. Burant, J. M. Millam, S. S. Iyengar, J. Tomasi, V. Barone, B. Mennucci, M. Cossi, G. Scalmani, N. Rega, G. A. Petersson, H. Nakatsuji, M. Hada, M. Ehara, K. Toyota, R. Ukuda, J. Hasegawa, M. Ishida, T. Nakajima, Y. Honda, O. Kitao, H. Nakai, M. Klene, X. Li, J. E. Knox, H. P. Hratchian, J. B. Cross, C. Adamo, J. Jaramillo, R. Gomperts, R. E. Stratmann, O. Yazyev, A. J. Austin, R. Cammi, C. Pomelli, J. W. Ochterski, P. Y. Ayala, K. Morokuma, G. A. Voth, P. Salvador, J. J. Dannenberg, V. G. Zakrzewski, S. Dapprich, A. D. Daniels, M. C. Strain, O. Farkas, D. K. Malick, A. D. Rabuck, K. Raghavachari, J. B. Foresman, J. V. Ortiz, Q. Cui, A. G. Baboul, S. Clifford, J. Cioslowski, B. B. Stefanov, G. Liu, A. Liashenko, P. Piskorz, I. Komaromi, R. L. Martin, D. J. Fox, T. Keith, M. A. Al-Laham, C. Y. Peng, A. Anayakkara, M. Challacombe, P. M. W. Gill, B. Johnson, W. Chen, M. W. Wong, C. Gonzalez and J. A. Pople, *Gaussian 03, Revision B.05*, Gaussian Inc., Pittsburgh, PA, 2003.
52 M. Brandbyge, J.-L. Mozos, P. Ordejón, J. Taylor and K. Stokbro, *Phys. Rev. B: Condens. Matter Mater. Phys.*, 2002, **65**, 165401.
53 J. Taylor, H. Guo and J. Wang, *Phys. Rev. B: Condens. Matter Mater. Phys.*, 2001, **63**, 121104.
54 Atomistix Toolkit, QuantumWise A/S, (www.quantumwise.com).
55 J. Taylor, H. Guo and J. Wang, *Phys. Rev. B: Condens. Matter Mater. Phys.*, 2001, **63**, 245407.
56 J. P. Perdew, K. Burke and M. Ernzerhof, *Phys. Rev. Lett.*, 1996, **77**, 3865.
57 Y. Meir and N. S. Wingreen, *Phys. Rev. Lett.*, 1992, **68**, 2512.
58 M. Büttiker, Y. Imry, R. Landauer and S. Pinhas, *Phys. Rev. B: Condens. Matter Mater. Phys.*, 1985, **31**, 6207.
59 M. Kiguchi and S. Kaneko, *Phys. Chem. Chem. Phys.*, 2013, **15**, 2253–2267.
60 G. C. Solomon, C. Herrmann, T. Hansen, V. Mujica and M. A. Ratner, *Nat. Chem.*, 2010, **2**, 223–228.
61 G. C. Solomon, C. Herrmann, J. Vura-Weis, M. R. Wasielewski and M. A. Ratner, *J. Am. Chem. Soc.*, 2010, **132**, 7887–7889.
62 R. Matsushita and M. Kiguchi, *Phys. Chem. Chem. Phys.*, 2015, **17**, 21254–21260.
63 H. Liu, Y. He, J. Zhang, J. Zhao and L. Chen, *Phys. Chem. Chem. Phys.*, 2015, **17**, 4558–4568.
64 V. Kaliginedi, A. V. Rudnev, P. Moreno-García, M. Baghernejad, C. Huang, W. Hong and T. Wandlowski, *Phys. Chem. Chem. Phys.*, 2014, **16**, 23529–23539.
65 C. Toher, A. Filippetti, S. Sanvito and K. Burke, *Phys. Rev. Lett.*, 2005, **95**, 146402.
66 R. B. Pontes, A. R. Rocha, S. Sanvito and A. Fazzio, A. o. J. R. da Silva, *ACS Nano*, 2011, **5**, 795–804.
67 A. de Melo Souza, I. Rungger, R. B. Pontes, A. R. Rocha, A. J. R. da Silva, U. Schwingenschlöegl and S. Sanvito, *Nanoscale*, 2014, **6**, 14495–14507.